Biogeosciences Discuss., 12, 7257–7299, 2015
www.biogeosciences-discuss.net/12/7257/2015/
doi:10.5194/bgd-12-7257-2015

Biogeosciences Discussions
Open Access

Nitrogen cycling in shallow low oxygen coastal waters off Peru from nitrite and nitrate nitrogen and oxygen isotopes

H. Hu[1,*], A. Bourbonnais[1,*], J. Larkum[1], H. W. Bange[2], and M. A. Altabet[1,*]

[1]School for Marine Science and Technology, University of Massachusetts Dartmouth, 706 South Rodney French Blvd, New Bedford, MA 02744-1221, USA
[2]GEOMAR Helmholtz Centre for Ocean Research Kiel, Düsternbrooker Weg 20, 24105 Kiel, Germany
[*]These authors contributed equally to this work.

Received: 17 April 2015 – Accepted: 20 April 2015 – Published: 18 May 2015

Correspondence to: A. Bourbonnais (abourbonnais@umassd.edu)

Published by Copernicus Publications on behalf of the European Geosciences Union.

Abstract

O_2 minimum zones (OMZ) of the world's oceans are important locations for microbial dissimilatory NO_3^- reduction and subsequent loss of combined nitrogen (N) to biogenic N_2 gas. This is particularly so when the OMZ is coupled to a region of high productivity leading to high rates of N-loss as found in the coastal upwelling region off Peru. Stable N isotope ratios (and O in the case of NO_3^- and NO_2^-) can be used as natural tracers of OMZ N-cycling because of distinct kinetic isotope effects associated with microbially-mediated N-cycle transformations. Here we present NO_2^- and NO_3^- stable isotope data from the nearshore upwelling region off Callao, Peru. Subsurface O_2 was generally depleted below about 30 m depth with O_2 less than 10 µM, while NO_2^- concentrations were high, ranging from 6 to 10 µM and NO_3^- was in places strongly depleted to near 0 µM. We observed for the first time, a positive linear relationship between NO_2^- $\delta^{15}N$ and $\delta^{18}O$ at our coastal stations, analogous to that of NO_3^- N and O isotopes during assimilatory and dissimilatory reduction. This relationship is likely the result of rapid NO_2^- turnover due to higher organic matter flux in these coastal upwelling waters. No such relationship was observed at offshore stations where slower turnover of NO_2^- facilitates dominance of isotope exchange with water. We also evaluate the overall isotope fractionation effect for N-loss in this system using several approaches that vary in their underlying assumptions. While there are differences in apparent fractionation factor (ε) for N-loss as calculated from the $\delta^{15}N$ of [NO_3^-], DIN, or biogenic N_2, values for ε are generally much lower than previously reported, reaching as low as 6.5 ‰. A possible explanation is the influence of sedimentary N-loss at our inshore stations which incurs highly suppressed isotope fractionation.

BGD
12, 7257–7299, 2015

1 Introduction

Chemically combined nitrogen (N, e.g. NO_3^-) is an important phytoplankton nutrient limiting primary productivity and carbon export throughout much of the ocean (e.g. Gruber, 2008). The marine nitrogen cycle involves a series of microbial processes, which transfer N between a number of chemical forms. These include N_2 fixation, nitrification (ammonium (NH_4^+) and nitrite (NO_2^-) oxidation), and loss of combined N to N_2 via denitrification and anammox. Of particular importance is the global balance between sources of combined N (N_2 fixation) and N-loss processes which ultimately control the combined N content of the ocean and thus its productivity and strength of the biological carbon pump. N-loss typically occurs under nearly anoxic conditions where the first step, dissimilatory NO_3^- reduction to NO_2^-, is used by heterotrophic microbes in lieu of oxygen (O_2) respiration for electron donation. Canonically, the denitrification pathway of successive reduction of NO_3^-, NO_2^-, nitric oxide (NO), nitrous oxide (N_2O) and finally N_2 was considered as the dominant pathway for N-loss. However there is considerable evidence for other pathways for N-loss, such as anammox ($NO_2^- + NH_4^+ \rightarrow N_2$; Kuypers et al., 2003, 2005; Lam et al., 2009). There is still considerable debate over the dominant pathways for N-loss, denitrification or anammox in Oxygen Minimum Zones (OMZ's) (e.g. Lam et al., 2009; Ward et al., 2009; Babbin et al., 2014). These processes vary in space and time and also likely depend on the quantity and quality of organic matter. It follows that there is still considerable uncertainty as to the controls on N-loss as well as the role for other linking processes such as DNRA (NO_3^- to NH_4^+) and NO_2^- oxidation in the absence of O_2.

Marine N-loss to N_2 occurs predominately in reducing sediments and the O_2 deficient water columns of OMZ's as found in the Arabian Sea and Eastern Tropical North and South Pacific. NO_2^- is an important intermediate during N-loss and generally accumulates at concentrations of up to $\sim 10\,\mu M$ in these regions. The depletion of NO_3^- is typically quantified as a dissolved inorganic N ($DIN = NO_3^-$, NO_2^- and NH_4^+) deficit relative to phosphate (PO_4^{-3}) assuming Redfield stoichiometry and the accumulation of

BGD
12, 7257–7299, 2015

biogenic N_2 (when measured) is detected as anomalies in N_2/Ar relative to saturation with atmosphere (Richards and Benson, 1961; Chang et al., 2010; Bourbonnais et al., 2015).

NO_3^- and NO_2^- N and O isotopes represent a useful tool to study N cycle transformations because biologically mediated reactions are generally faster for lighter isotopes. For example, both assimilatory and dissimilatory NO_3^- reduction produces a strong enrichment in both ^{15}N ($\delta^{15}N = [(^{15}N/^{14}N_{sample})/(^{15}N/^{14}N_{standard}) - 1] \times 1000$) and ^{18}O ($\delta^{18}O = [(^{18}O/^{16}O_{sample}) / (^{18}O/^{16}O_{standard}) - 1] \times 1000$) in the residual NO_3^- (Cline and Kaplan, 1975; Brandes et al., 1998; Voss et al., 2001; Granger et al., 2004, 2008; Sigman et al., 2005).

Canonical values for the N isotope effect ($\varepsilon \approx \delta^{15}N_{substrate} - \delta^{15}N_{product}$, at no significant substrate depletion) associated with microbial NO_3^- reduction during water-column denitrification are ranging from 20 to 30‰ (Brandes et al., 1998; Voss et al., 2001; Granger et al., 2008). In contrast, the isotope effect of sedimentary denitrification is highly suppressed in the water-column (generally < 3‰) mostly due to near complete consumption of the porewater NO_3^- and diffusion limitation (Brandes and Devol, 1997; Lehmann et al., 2007; Alkhatib et al., 2012). The $\delta^{15}N$ and $\delta^{18}O$ of NO_3^- are affected in fundamentally different ways during NO_3^- consumption and production processes. The ratio of the ^{15}N and ^{18}O fractionation factors ($^{18}\varepsilon : {}^{15}\varepsilon$) during NO_3^- consumption during denitrification or assimilation by phytoplankton in surface waters is close to 1:1 (Casciotti et al., 2002; Granger et al., 2004, 2008). While the $\delta^{15}N$ of the newly nitrified NO_3^- depends on the $\delta^{15}N$ of the precursor molecule being nitrified, the O atom is mostly derived from water (with a $\delta^{18}O$ of ~ 0‰), with significant isotopic fractionation associated with O incorporation during NO_2^- and NH_4^+ oxidation (Casciotti, 2002; Buchwald and Casciotti, 2010; Casciotti et al., 2010). Therefore, any deviation from this 1:1 ratio in the field has been interpreted as evidences that NO_3^- regeneration is co-occurring with NO_3^- consumption (Sigman et al., 2005; Casciotti and McIlvin, 2007; Bourbonnais et al., 2009). Additional information on N-cycling processes can be ob-

BGD
12, 7257–7299, 2015

tained from the isotopic composition of NO_2^-. For example, NO_2^- oxidation is atypically associated with an inverse N isotope effect (Casciotti, 2009) which results in a lower NO_2^- $\delta^{15}N$ than initially produced by NH_4^+ oxidation and NO_3^- reduction (Casciotti and Buchwald, 2012). NO_2^- reduction would be expected to produce an analogous relationship between $\delta^{15}N$-NO_2^- and $\delta^{18}O$-NO_2^- as for NO_3^- consumption, though there are no observations in the literature. However, NO_2^-O isotope exchange with water (as a function of pH and temperature) would reduce the slope of a NO_2^- $\delta^{18}O$ vs. $\delta^{15}N$ relationship toward zero. NO_2^-turnover time can therefore be assessed from this observed relationship and in situ pH and temperature (Buchwald and Casciotti, 2013).

It is still under discussion whether the global ocean N budget is in balance, with current estimates indicating a large fixed N deficit of up to $> 400\,Tg\,year^{-1}$ (Gruber, 2004; Codispoti, 2007). Large uncertainties are associated with this budget, mainly in constraining the proportion of sedimentary denitrification, which is typically estimated from ocean's N isotope balance and the expressed isotope effects for water-column vs. sedimentary NO_3^- reduction during denitrification (e.g. Brandes and Devol, 2002; Altabet, 2007). Liu (1979) was first to suggest a lower ε for N-loss in the Peru OMZ as compared to the subsequently accepted canonical range. Ryabenko et al. (2012) provided a more widely distributed set of data in support. Most recently, a detailed study in a region of extreme N-loss associated with a Peru coastal mode-water eddy confirmed a value for ε for N-loss of ~ 14 ‰ (Bourbonnais et al., 2015). Applying such a lowered value to global budgets would bring the global N budget closer to balance.

Ryabenko et al. (2012) also suggested that ε values were even lower in the shelf region of the Peru OMZ. To investigate further, we present here N and O of NO_2^- and NO_3^- isotope data from shallow coastal waters near Callao, off the coast of Peru. O_2 was generally depleted to near 0 µM below 30 m, while NO_2^- concentrations were high. These waters are highly productive as a consequence of active upwelling that is also responsible for shoaling of the oxycline. We also observe for the first time, a positive relationship between NO_2^- $\delta^{15}N$ and $\delta^{18}O$ that is likely the result of NO_2^- reduction

BGD
12, 7257–7299, 2015

and analogous to the well-known relationship for assimilatory and dissimilatory NO_3^- reduction. No such relationship is observed at offshore stations. We also observe fairly low overall isotope effects for N-loss as compared to canonical values. Our derived isotope effects for N-loss are even lower than recently reported for an offshore eddy in the same region observed during the same time period as our study (Bourbonnais et al., 2015). We infer the likely influence of sedimentary N-loss at our relatively shallow sites, which incurs a highly suppressed isotope effect.

2 Material and methods

2.1 Sampling

The R/V *Meteor* 91 research cruise (M91) to the eastern tropical South Pacific Ocean off Peru in December 2012 was part of the SOPRAN program (Surface Ocean Processes in the Anthropocene: www.sopran.pangaea.de) and the German SFB 754 project (Climate–Biogeochemistry Interactions in the Tropical Ocean: www.sfb754.de). It included an along shore transect of seven inner shelf stations located between 12 to 14° S that were chosen for this study (Fig. 1). These stations had a maximum depth of 150 m except for station 68 (250 m depth). During this time period, there was active coastal upwelling as seen by relatively low satellite sea surface temperature and higher chlorophyll a concentrations along the shore (Fig. 1). Samples for NO_3^- and NO_2^- isotopic composition and N_2/Ar ratio were collected using Niskin bottles mounted on a CTD/Rosette system, which was equipped with pressure, temperature, conductivity and oxygen sensors. Oxygen (O_2) and nutrients concentrations were also measured on board using standard methods as described in Stramma et al. (2013).

BGD
12, 7257–7299, 2015

2.2 NO_2^- and NO_3^- isotope analysis

NO_2^- samples were collected and stored in 125 mL HDPE bottles preloaded with 2.25 mL 6 M NaOH to prevent microbial activity as well as alteration of δ^{18}O-NO_2^- by isotope exchange with water (Casciotti et al., 2007). Bottles were kept frozen after sample collection, though we have subsequently determined in the laboratory that seawater samples preserved in this way can be kept at room temperature for at least a year without alteration of NO_2^- δ^{15}N or δ^{18}O (unpublished data). Samples were analyzed by continuous He flow isotope-ratio mass spectrometry (CF-IRMS; see below) after chemical conversion to N_2O using acetic acid buffered sodium azide (McIlvin and Altabet, 2005). Because of high sample pH, the reagent was modified for NO_2^- isotope analysis by increasing the acetic acid concentration to 7.84 M resulting in a final concentration of 418 mM in the sample. Calibration standards used were N23, N7373, and N10219 (see Casciotti and McIlvin, 2007).

NO_3^- samples were collected in 125 mL HDPE bottles preloaded with 1 mL of 2.5 mM sulfamic acid in 25 % HCl to both act as a preservative and to remove NO_2^- (Granger and Sigman, 2009). Samples were also kept at room temperature and we have found that they can be stored in this way for many years without alteration of NO_3^- δ^{15}N or δ^{18}O. Cadmium reduction was used to convert NO_3^- to NO_2^- prior to conversion to N_2O and IRMS analysis also using the "azide method" (McIlvin and Altabet, 2005). Standards for NO_3^- isotope analysis were N3, USGS34 and USGS35 (Casciotti et al., 2007). The lowest concentration of NO_2^- or NO_3^- analyzed for isotopic composition was 0.5 µM.

A GV Instruments IsoPrime IRMS coupled to an on-line He continuous-flow purge/trap preparation system was used for isotope analysis (Sigman et al., 2001; Casciotti et al., 2002; McIlvin and Altabet, 2005). N_2O produced by the azide reaction was purged with He from the septum sealed 20 mL vials and trapped and cryofocused using a sequence of two liquid nitrogen traps. A combination of Nafion membrane, chemical traps, cryotraps, and a capillary GC column was used to purify the N_2O prior

BGD
12, 7257–7299, 2015

to transfer to the IRMS. Total run time was 700 s sample^{-1} (McIlvin and Altabet, 2005). Isotopic values are referenced against atmospheric N_2 for $\delta^{15}N$ and VSMOW for $\delta^{18}O$. Reproducibility was 0.2 ‰ and 0.5 ‰, respectively.

2.3 N_2/Ar IRMS analysis and calculation of biogenic N_2

The accumulation of biogenic N_2 from denitrification and anammox can be measured directly from precise N_2/Ar measurements (see above; Richards and Benson, 1961; Chang et al., 2010; Bourbonnais et al., 2015). As described in Charoenpong et al. (2014), N_2/Ar samples were collected from Niskin bottles using 125 mL serum bottles, and all samples were treated with $HgCl_2$ as a preservative and filled without headspace. When cavitation bubbles formed from cooling of warm, near-surface samples, these bubbles were collapsed and reabsorbed by warming in the laboratory to 30 to 35° C in a water bath before analysis. N_2/Ar was measured using an automated dissolved gas extraction system coupled to a multicollector IRMS (Charoenpong et al., 2014). Excess N_2 was calculated first from anomalies relative to N_2/Ar expected at saturation with atmosphere at in situ temperature and salinity. Locally produced biogenic N_2 was obtained by subtracting excess N_2 at the corresponding density surface for waters outside of the OMZ (O_2 > 10 µM) not affected by N-loss (Chang et al., 2010; Bourbonnais et al., 2015). Reproducibility was better than 0.7 µM for excess N_2 and 0.03 ‰ for $\delta^{15}N$-N_2. $\delta^{15}N$ of biogenic N_2 was calculated by mass balance as in Bourbonnais et al. (2015).

2.4 Isotope effect (ε) calculations

Isotope effects are estimated using the Rayleigh equations describing the change in isotope ratio as a function of fraction of remaining substrate. For the closed system

BGD
12, 7257–7299, 2015

forms of these equations (Mariotti et al., 1981):

$$\delta^{15}\text{N-NO}_3^- = \delta^{15}\text{N-NO}_3^-(f = 1) - \varepsilon \times \ln[f_1] \text{ or}$$
$$\delta^{15}\text{N-DIN} = \delta^{15}\text{N-DIN}(f = 1) - \varepsilon \times \ln[f_2] \quad (1)$$

where f_1 is the fraction of remaining NO_3^- and f_2 is the fraction of remaining DIN ($[NO_3^-]$ + $[NO_2^-]$). δ^{15}N-DIN is the average δ^{15}N for NO_3^- and NO_2^- weighted by their concentrations. The fraction of remaining DIN is a better estimation of the overall isotope effect for N-loss (Bourbonnais et al., 2015), while using NO_3^- as the basis to calculate ε specifically targets NO_3^- reduction. See below for details of f value calculation.

The overall isotope effect for N-loss can also be estimated from the δ^{15}N of biogenic N_2 produced:

$$\delta^{15}\text{N-biogenic } N_2 = \delta^{15}\text{N-DIN}(f = 1) + \varepsilon \times f_2/[1 - f_2] \times \ln[f_2] \quad (2)$$

Whereas the closed system equations assume no addition or loss of substrate or product, corresponding steady-state open system equations can account for such effects (Altabet, 2005):

$$\delta^{15}\text{N-NO}_3^- = \delta^{15}\text{N-NO}_3^-(f = 1) + \varepsilon \times [1 - f_1] \text{ or}$$
$$\delta^{15}\text{N-DIN} = \delta^{15}\text{N-DIN}(f = 1) + \varepsilon \times [1 - f_2] \quad (3)$$
$$\delta^{15}\text{N-biogenic } N_2 = \delta^{15}\text{N-DIN}(f = 1) - \varepsilon \times f_2 \quad (4)$$

For all equations, the slope represents ε and the y-intercept is the initial δ^{15}N prior to N-loss. For calculations using equations 2 and 4 we only used δ^{15}N values associated with biogenic N_2 greater than 7.5 µM because of increasing noise with small levels of biogenic N_2 (up to 20 µM in this study) over the huge atmospheric dissolved N_2 background (typically up to ~ 500 µM) as in Bourbonnais et al. (2015).

BGD
12, 7257–7299, 2015

Since the closed system equations assume no loss or resupply of substrate or production in a water parcel, they are appropriate where there is little mixing and/or advection is dominant over mixing. The open system equations take into account supply from or loss to surrounding water parcel, e.g. mixing dominance. Both cases represent extreme situations. For our inshore water stations, where we observed a single water mass (Fig. 2), a closed system should be a more realistic approximation of ε. In the next section, we will estimate and compare ε using both sets of equations.

To do so, we need to estimate the fraction of NO_3^- or DIN remaining (f). The assumption of Redfield stoichiometry (as in Eq. 6) in source waters is typically made:

$$f_{1p} = [NO_3^-]/Np_{expected} \text{ or } f_{2p} = ([NO_3^-] + [NO_2^-])/Np_{expected} \quad (5)$$

$$Np_{expected} = 15.8 \times ([PO_4^{3-}] - 0.3) \quad (6)$$

$$N_{observed} = [NO_3^-] + [NO_2^-] + [NH_4^+] \quad (7)$$

Equation (6) was derived in Chang et al. (2010) from stations to the west of the ETSP OMZ (143–146° W) and takes into account preformed nutrient concentrations. In our study, NH_4^+ generally did not significantly accumulate, except at station 63, and was thus not included. This has also been a traditional approach to quantify N-loss in OMZ's (N deficit) by comparing observed [DIN] to concentrations expected assuming Redfield stoichiometry:

$$Np_{def} = Np_{expected} - N_{observed} \quad (8)$$

However the assumption of Redfield stoichiometry may not be appropriate in this shallow environment due to preferential release of PO_4^{3-} following iron and manganese oxyhydroxide dissolution in anoxic sediments (e.g. Reed et al., 2011). An alternative method of calculating f makes use of our biogenic N_2 measurements to estimate ex-

BGD
12, 7257–7299, 2015

pected N prior to N-loss ($N_{expected}$ bio N_2) and f values based on it:

$$N_{expected}\,\text{bio}\,N_2 = [NO_3^-] + [NO_2^-] + 2 \times [\text{Biogenic}\,N_2] \quad (9)$$

$$f_{1bioN2} = [NO_3^-]/N_{expected}\,\text{bio}\,N_2 \text{ or}$$

$$f_{2bioN2} = [NO_3^- + NO_2^-]/N_{expected}\,\text{bio}\,N_2 \quad (10)$$

A third way to estimate f is to use NO_3^- or DIN concentrations divided by observed maximum $[NO_3^-]$ or [DIN].

3 Results

3.1 Hydrographic characterization

A common T–S relationship was found indicating a common source of water upwelling at these inner shelf stations (Fig. 2). This is expected as in these coastal, shallow waters, wind-driven surface currents play a dominant role. The upwelled water appears to be a single water mass with low O_2 and high nutrients originating from the offshore OMZ. O_2 increased only in warmer near-surface waters as a consequence of atmospheric exchange. There was a change in surface water temperature from 15 to 20 °C (Fig. 1b) with distance along the coast (from 12.0 to 14.0° S, about 222 km) that indicates corresponding changes in upwelling intensity. Stronger local wind forcing likely brought up colder deep water near station 63.

3.2 Dissolved O_2 and nutrient concentrations

As a consequence of active upwelling sourced from the offshore OMZ, the oxycline was very shallow at our in-shore stations. O_2 was generally depleted below 10 to 20 m (Fig. 3a) and was always less than 10 µM below 30 m. As we are focusing on N-transformations that occur in the absence of O_2, our data analyses will be mainly

BGD
12, 7257–7299, 2015

restricted to samples where $[O_2]$ is below this value. Whereas a recent study indicates that denitrification and anammox are reversibly suppressed at nanomolar O_2 levels (Dalsgaard et al., 2014), CTD deployed O_2 sensors are not sufficiently sensitive to detect such low concentrations and hence our choice of a 10 µM threshold. Both $Si(OH)_4$ and PO_4^{3-} concentrations had very similar vertical and along section distributions (Fig. 3). Concentrations were at a minimum at the surface, presumably due to phytoplankton uptake, and increased with depth to up to 46 and 3.7 µM, respectively. Station 63 had the highest near-bottom concentrations, a likely result of local intense upwelling as suggested by higher chlorophyll *a* concentrations (Fig. 1) and/or from release from the sediments. The latter is suggested by high near-bottom $[NH_4^+]$ (up to ~ 4 µM) as compared to the other stations (Fig. 3b–d).

In contrast to other nutrients, $[NO_3^-]$ and $[NO_2^-]$ were lowest near-bottom at station 63, only reaching their maxima above 60 m. Across most of our stations, $[NO_3^-]$ was 22 µM at 20 to 40 m depth but decreased to near zero deeper within the O_2-depleted zone due to microbially mediated N-loss (Fig. 4a). $[NO_2^-]$ correspondingly ranged from 6 to 11 µM for $[O_2] < 10$ µM (Fig. 4b). The highest $[NO_2^-]$ (11 µM) was found at around 50 m (station 64), but only reached 6 µM at all other stations.

3.3 NO_2^- and NO_3^- isotope compositions

As a consequence of kinetic isotope fractionation during N-loss, the N and O isotope composition of NO_3^- and NO_2^- varied inversely with $[NO_3^-]$ and $[NO_2^-]$ with maximum $\delta^{15}N$ and $\delta^{18}O$ values near the bottom at each station. $\delta^{15}N\text{-}NO_3^-$ increased from about 10 ‰ in surface waters to up to about 50 ‰ in the O_2-depleted zone (Fig. 4c), with near bottom values at station 64 significantly higher (50 ‰) than at the other stations which ranged from 20 to 30 ‰. $\delta^{15}N\text{-}NO_2^-$ varied from –25 to about 10 ‰ (Fig. 4d) with maximum values also in deeper waters at station 64. Due to very low $[NO_3^-]$ and $[NO_2^-]$, $\delta^{15}N\text{-}NO_3^-$ and $\delta^{15}N\text{-}NO_2^-$ could not be measured below 37 m at station 63.

BGD
12, 7257–7299, 2015

As expected for N-loss, δ^{18}O-NO_3^- positively co-varied with δ^{15}N-NO_3^- and ranged from 12 to 46 ‰. We observed an overall linear relationship between δ^{15}N-NO_3^- and δ^{18}O-NO_3^- with a slope of 0.86 and an *y*-intercept of 1.90 (r^2 = 0.996, see Fig. 5a). NO_3^- δ^{15}N and δ^{18}O have been shown to increase equally (ratio 1:1) during assimilatory and dissimilatory NO_3^- reduction (Casciotti et al., 2002; Sigman et al., 2003). However, deviations from this trend have been observed in the ocean and interpreted as evidence for co-occurring NO_3^- production processes (Sigman et al., 2005; Casciotti and McIlvin, 2007; Bourbonnais et al., 2009, 2015). In this study, we observed a NO_3^- δ^{18}O vs. δ^{15}N relationship less than 1, likely originating from NO_2^- re-oxidation to NO_3^- in our environmental setting as in Casciotti and McIlvin (2007). We also observed, for the first time, a significant correlation between δ^{15}N-NO_2^- and δ^{18}O-NO_2^- in the OMZ for our in-shore water stations (Fig. 5b). As in prior studies (Casciotti and McIlvin, 2007; Casciotti et al., 2013), no such relationship was observed by us for a nearby set of offshore stations (see Fig. 5c) where longer NO_2^- turnover times likely facilitated O isotope exchange with water. We will discuss implications of this unique finding in the next section.

3.4 Isotope effect (ε)

Isotope effects were calculated using Eqs. (1) to (4) to compare closed vs. open system assumptions as well as different approaches to estimating *f*. Examples of plots of the closed system equations, with *f* calculated using biogenic N_2 are shown in Fig. 6. Comparison of results using all 3 approaches for calculating *f* (i.e. Redfield stoichiometry, biogenic N_2 and observed substrate divided by maximum "upwelled" concentration, (see Sect. 2.4) are shown in Tables 1 (closed system) and 2 (open system). In the case of the closed system, ε values were in all cases lower than canonical, ranging narrowly from about 6 ‰ for changes in the δ^{15}N of DIN to about 14 ‰ for changes in δ^{15}N-NO_3^- (Table 1). For the open system equations, estimated ε was higher and covered a large

BGD
12, 7257–7299, 2015

and unrealistic range from about 12 ‰ for changes in the biogenic N_2 to about 63 ‰, respectively for changes in the $\delta^{15}N$ of NO_3^-. The Rayleigh equation's *y*-intercepts where $f = 1$, represent the initial $\delta^{15}N$ of NO_3^- or DIN and varied from −0.5 to 3.7 ‰ and −18.4 to 6.2 ‰ for the closed and open systems, respectively. The higher end of this range is more realistic based on prior isotopic measurements for source waters.

3.5 The $\delta^{15}N$ difference between NO_3^- and NO_2^-

The difference in $\delta^{15}N$ between NO_3^- and NO_2^- ($\Delta\delta^{15}N$) reflect the combined isotope effects of simultaneous NO_3^- reduction, NO_2^- reduction, and NO_2^- oxidation. For NO_3^- reduction alone, highest $\Delta\delta^{15}N$ values would be around 25 ‰ at steady-state (Cline and Kaplan, 1975; Brandes et al., 1998; Voss et al., 2001; Granger et al., 2004, 2008; Sigman et al., 2005). The effect of NO_2^- reduction would be to increase the $\delta^{15}N$ of the residual NO_2^-, decreasing $\Delta\delta^{15}N$. In contrast, NO_2^- oxidation is associated with an inverse kinetic isotope effect (Casciotti, 2009) and would act to decrease the residual $\delta^{15}N$ of NO_2^- while concomitantly increasing the $\delta^{15}N$ of the NO_3^- pool, and hence overall increases the $\Delta\delta^{15}N$. Therefore, following NO_2^- oxidation, $\Delta\delta^{15}N$ may be larger than expected from NO_3^- and NO_2^- reduction alone, especially if the system is not at steady-state (Casciotti et al., 2013). $\Delta\delta^{15}N$ ranged from 15 ‰ to 40 ‰ (average = 29.78 ‰ and median = 32.5 ‰ ; Fig. 7) for samples with $O_2 < 10$ µM. These results confirm the presence of NO_2^- oxidation for at least some of our depth intervals.

3.6 N deficit, biogenic N_2 and $\delta^{15}N{-}N_2$

N deficits, biogenic N_2 concentrations, and $\delta^{15}N{-}N_2$ anomalies relative to equilibrium with atmosphere were overall greater in the O_2-depleted zone reaching highest values near the bottom of station 63 (Fig. 8). N deficit, calculated assuming Redfield stoichiometry (Eqs. 6–8), ranged from 17 to 59 µM in this region. The concentration of biogenic N in N_2 ranged from 12 to 36 µM-N and, as expected, was strongly linearly correlated

BGD
12, 7257–7299, 2015

with N deficit (r^2 = 0.87; Fig. 9c). However, the slope of 0.45 for the linear relationship shows biogenic N in N_2 to be only half that expected from Np_{def}, as a possible consequence of excess PO_4^{-3}. The linear relationship (r^2 = 0.91) observed between biogenic N in N_2 and DIN (Fig. 9a) supports a single initial DIN value for the source waters to our stations and the validity of using this as a basis for calculating f. The slope of the correlation (0.74) is much closer to 1 as compared to the correlation with Np_{def}, further supporting excess [PO_4^{-3}] as a contributor to the latter. However this value is still significantly less than 1, suggesting that biogenic N in N_2 may also be underestimated. Because our data are restricted to O_2-depleted depths, it is unlikely that biogenic N_2 was lost to the atmosphere. Alternatively, mixing of water varying in N_2/Ar can result in such underestimates of biogenic N_2 when N_2/Ar anomalies are used to calculate excess N_2 (see Charoenpong et al., 2014). As seen below, though, our estimates of ε are rather insensitive to choice of Np_{def}, biogenic N in N_2, or DIN concentration changes as the basis for calculation of f.

The $\delta^{15}N\text{-}N_2$ anomaly, derived as in Charoenpong et al. (2014), ranged from −0.2 to 0.1 ‰ (Fig. 8c). This signal appears small as compared to the isotopic composition of NO_3^- and NO_2^- but is (1) analytically significant and (2) the result of dilution by the large background of atmospheric N_2 (800 to 1000 µM N in N_2).

4 Discussion

4.1 Behavior of NO_2^-

NO_2^- is an important intermediate during either oxidative or reductive N-cycle pathways and can accumulate at low concentrations through the ocean. While NO_2^- is generally elevated at the base of the sunlit euphotic zone (i.e. primary NO_2^- maximum; Dore and Karl, 1996; Lomas and Lipschultz, 2006), highest concentrations are found in OMZ's as part of the secondary NO_2^- maximum (Codispoti and Christensen, 1985;

BGD
12, 7257–7299, 2015

Lam et al., 2011). Accordingly, relatively high [NO_2^-] (7.2 to 10.7 µM) was observed at 50–75 m depth in coastal O_2-depleted waters in this study as a likely consequence of dissimilatory NO_3^- reduction (e.g. Codispoti et al., 1986). Though relatively shallow, the high NO_2^- is functionally equivalent to a secondary NO_2^- maximum as it is a likely consequence of intense coastal upwelling bringing O_2-depleted, NO_2^--rich waters near surface.

Several processes can influence the isotopic composition of NO_2^-. NO_3^- reduction to NO_2^- is associated with a ε of 20 to 30 ‰ (Cline and Kaplan, 1975; Brandes et al., 1998; Voss et al., 2001; Granger et al., 2004, 2008; Sigman et al., 2005) and acts to produce NO_2^- depleted in ^{15}N and ^{18}O. In contrast, NO_2^- reduction as part of either anammox, denitrification or DNRA increases both the $\delta^{15}N$ and $\delta^{18}O$ of residual NO_2^-, with laboratory and field estimates for ε clustering around 12 ‰ to 16 ‰ (Bryan et al., 1983; Brunner et al., 2013; Bourbonnais et al., 2015). However, NO_2^- oxidation to NO_3^- at low or non-detectable [O_2] have been shown to be an important sink for NO_2^- in OMZs (e.g. Füssel et al., 2012). Anammox bacteria can also use NO_2^- as an electron donor during CO_2 fixation under anaerobic conditions (Strous et al., 2006). NO_2^- oxidation incurs an unusual inverse N isotope effect varying from −13 ‰ for aerobic (Casciotti, 2009) to −30 ‰ for anammox-mediated (Brunner et al., 2013) NO_2^- oxidation, resulting in lower $\delta^{15}N$ for NO_2^- as it is oxidized to NO_3^-.

To assess the influence of the various N cycle processes that have NO_2^- as either a substrate or product, we first examined the relationship between the $\delta^{15}N$ and $\delta^{18}O$ of NO_2^-. Regarding the latter, past studies have found NO_2^- $\delta^{18}O$ values in OMZ's in isotope equilibrium with water as a likely consequence of relatively long turnover time. O isotope exchange involves the protonated form, HNO_2, but because of its high pKa as compared to NO_3^-, this process can occur even at neutral to alkaline ocean pH on a time scale of 2 to 3 months at environmentally relevant temperatures (Casciotti et al., 2007). NO_2^- $\delta^{18}O$ isotopic composition at equilibrium with water is a function of the $\delta^{18}O$ of water and temperature (+14 ‰ for seawater at 22 °C; Casciotti et al., 2007;)

BGD
12, 7257–7299, 2015

and independent of its $\delta^{15}N$ value such that plots of NO_2^- $\delta^{18}O$ vs. $\delta^{15}N$ usually have a slope of near zero. This is seen in our NO_2^- data from offshore stations occupied during M90 (Fig. 5).

If NO_2^- turnover was faster than equilibration time with water, NO_3^- and NO_2^- reduction should also produce a positive relationship between NO_2^- $\delta^{15}N$ and $\delta^{18}O$. Coupled $\delta^{15}N$ and $\delta^{18}O$ effects for NO_2^- have not been as well studied as for NO_3^-. Nevertheless, NO_2^- reduction whether part of the denitrification, anammox or DNRA pathways, would likely linearly increase both NO_2^- $\delta^{15}N$ and $\delta^{18}O$, but the corresponding slopes are not yet known. NO_2^- oxidation has its own unique set of isotope effects (Casciotti, 2009; Buchwald and Casciotti, 2010). Because of the inverse ^{15}N isotope fractionation effect during NO_2^- oxidation, $\Delta\delta^{15}N$ will increase by driving the $\delta^{15}N$ of NO_2^- to lower values and the $\delta^{15}N$ of NO_3^- to higher values (Casciotti, 2009). It also alters the NO_3^- $\delta^{18}O:\delta^{15}N$ relationship since the added O atom is mostly derived from water (e.g. Andersson and Hooper, 1983) with a $\delta^{18}O$ of ~ 0 ‰. Moreover, enzyme catalysis associated with NO_2^- oxidation is readily reversible (Friedman et al., 1986) also causing O isotope exchange between NO_2^- and water (Casciotti et al., 2007). O atom incorporation during both NH_4^+ and NO_2^- oxidation have been shown to occur with significant isotope effect, such that the $\delta^{18}O$ of newly microbially produced NO_3^- in the ocean range from ~ -8 to -1 ‰ (Casciotti et al., 2010; Buchwald and Casciotti, 2010).

We observed, for the first time, a significant linear relationship for NO_2^- $\delta^{18}O$ vs. $\delta^{15}N$ at our inshore stations (slope $= 0.64 \pm 0.07$, $r^2 = 0.59$, p value $= 3 \times 10^{-6}$) where $O_2 < 10$ µM (Fig. 5b). In contrast to our offshore stations (Fig. 5c), this positive relationship demonstrates that the oxygen isotopic composition of NO_2^- is not in equilibrium with water due to both rapid NO_2^- turnover and the dominance of NO_2^- reduction over oxidation in Peru coastal waters as compared to offshore. More rapid N-loss (e.g. higher rates) has been reported in shallow waters off Peru presumably due to increased coastal primary production and organic matter supply to the in-shore OMZ (e.g. Codis-

BGD
12, 7257–7299, 2015

poti et al., 1986; Kalvelage et al., 2014), which could explain this more rapid NO_2^- turnover.

In principal, we can estimate NO_2^- turnover time from knowledge of rates for exchange with water and assumptions of the $\delta^{18}O$ vs. $\delta^{15}N$ slope expected in the absence of exchange. Unfortunately, the slope of the relationship between NO_2^- $\delta^{18}O$ vs. $\delta^{15}N$ expected in the absence of equilibration with water is not yet known. However, an upper limit for turnover time for NO_2^- can be estimated based on equilibration time as a function of in situ pH and temperature (Buchwald and Casciotti, 2013). During the M91 cruise in December, subsurface temperature was 13 to 15 °C along our transect and corresponding pH was near 7.8 (Michelle Graco, unpublished data). Assuming the NO_2^- pool is in steady-state, we estimated an equilibration time of ~ 40 days for pH near 7.8 (see Fig. 2 in Buchwald and Casciotti, 2013). A turnover time as low as 40 days implies a flux of N through the NO_2^- pool of up to 0.21 μM d^{-1}, as estimated from the maximum [NO_2^-] divided by this estimated turnover time. Assuming steady-state, this range also approximates the rates of NO_3^- reduction as well as NO_2^- oxidation plus production of N_2 from NO_2^-. This estimated flux is consistent with measured high NO_3^- reduction and NO_2^- oxidation rates of up to ~ 1 μM d^{-1} in Peru coastal waters (< 600 m depth, Kalvelage et al., 2013).

NO_2^- oxidation is a chemoautotrophic process that requires a thermodynamically favorable electron acceptor such as O_2. As mentioned above, NO_2^- oxidation appears to occur in OMZ's at low or non-detectable [O_2] (e.g. Füssel et al., 2012) despite lack of knowledge of its thermodynamically favorable redox couple. The difference in $\delta^{15}N$ between NO_2^- and NO_3^- ($\Delta\delta^{15}N = \delta^{15}N\text{-}NO_3^- - \delta^{15}N\text{-}NO_2^-$ see Sect. 3.3) is further evidence for the presence of NO_2^- oxidation in the OMZ (e.g. Casciotti et al., 2013). At steady-state, and in the absence of NO_2^- oxidation, $\Delta\delta^{15}N$ should be no more than the ε for NO_3^- reduction (20 to 30 ‰) minus the ε for NO_2^- reduction by denitrifying or anammox bacteria (12–16 ‰; Bryan et al., 1983; Brunner et al., 2013; Bourbonnais

BGD
12, 7257–7299, 2015

et al., 2015) or 8 to 18 ‰. Our results range from 15 ‰ to 40 ‰ and averaging 29.8 ‰ for samples with $O_2 < 10\,\mu M$ (Fig. 7).

The inverse kinetic isotope effect (Casciotti, 2009; Brunner et al., 2013) associated with NO_2^- oxidation is likely responsible for these high $\Delta\delta^{15}N$ values (e.g. Casciotti and Buchwald, 2012; Casciotti et al., 2013). Taking all isotope effects into account, the following equation can be derived to estimate $\Delta\delta^{15}N$ at steady-state:

$$\Delta\delta^{15}N(\text{steady state}) = \varepsilon_{NO_3\text{-red}} - (1-\gamma) \times \varepsilon_{NO_2\text{-red}} - \gamma \times \varepsilon_{NO_2\text{-oxid}} \quad (11)$$

where γ is the fraction of NO_2^- oxidized back to NO_3^-. Highest values (over 30 ‰) are found between 50 and 100 m (Fig. 7), implying greater importance for NO_2^- oxidation in deeper waters.

Given that $\varepsilon_{NO_2\text{-oxid}}$ has been reported to be −13 ‰ for aerobic NO_2^- oxidation and using the literature ranges for $\varepsilon_{NO_2\text{-red}}$ and $\varepsilon_{NO_2\text{-red}}$ above, our observed $\Delta\delta^{15}N$ implies that up to 100 % of NO_2^- produced by NO_3^- reduction could be oxidized back to NO_3^-. Alternatively, NO_2^- oxidation also occurs as part of the overall metabolism of anammox bacteria (Strous et al., 2006) which can be the dominant N_2 producers in the Peru OMZ (Kalvelage et al., 2013). A large inverse kinetic ε for NO_2^- oxidation of ~ −30 ‰ has been observed for anammox bacteria in culture (Brunner et al., 2013). If the sole pathway for NO_2^- oxidation, our data suggests NO_2^- oxidation up to only ~ 80 % of total NO_3^- reduction.

The deviations from a 1 : 1 relationship for NO_3^- $\delta^{18}O$ and $\delta^{15}N$ can also be indicative of NO_2^- oxidation. During assimilative or dissimilative NO_3^- reduction, NO_3^- $\delta^{15}N$ and $\delta^{18}O$ increase equally with a ratio of 1 : 1 (Granger et al., 2004, 2008). We observed a slope of about 0.86 (Fig. 5a) for the relationship for NO_3^- $\delta^{18}O$ vs. $\delta^{15}N$ in the inshore Peru OMZ, similar to recent off-shore observations (Bourbonnais et al., 2015). Prior reports of deviations toward higher values for the slope were indicative of addition of newly nitrified NO_3^- from a relatively low $\delta^{15}N$ source (e.g. see Sigman et al., 2005; Bourbonnais et al., 2009). Our observed deviation toward lower slope can instead be

BGD
12, 7257–7299, 2015

explained by the addition of newly nitrified NO_3^- with higher $\delta^{15}N$ relative to its $\delta^{18}O$, due to the inverse kinetic ε for NO_2^- oxidation. In fact, a slope for $\delta^{18}O:\delta^{15}N$ of either greater or less than 1 can be observed, depending on environmental NO_3^- isotopic composition relative to any in-situ sources. Casciotti and Buchwald (2012) showed model results where NO_2^- oxidation generally produces a slope < 1 for the NO_3^- $\delta^{18}O$ vs. $\delta^{15}N$ relationship, when the NO_3^- $\delta^{15}N$ and $\delta^{18}O$ are higher than about 15 ‰ as we have observed (Bourbonnais et al., 2015).

4.2 Isotope effects for N-loss

As described above, the Rayleigh fractionation equations (Eqs. 1–4) are used here to estimate ε values (Mariotti et al., 1981; Altabet, 2005) and examine the significance of calculations using (a) different approaches for calculating f (Eqs. 5 and 10), (b) changes in the $\delta^{15}N$ of substrate (DIN) vs. changes in the $\delta^{15}N$ of product (biogenic N_2), and (c) closed vs. open system equations. This approach provides redundancy in our estimates of ε and tests implied assumptions including N and ^{15}N balance between NO_3^- or DIN loss and the accumulation of biogenic N_2.

Linear regression coefficients for $\delta^{15}N$ (NO_3^-, DIN or biogenic N_2) vs. $\ln f$, $f/[1-f]\times \ln f$, $1-f$, or f as appropriate are listed in Tables 1 and 2. For illustration, example Rayleigh closed system plots for $\delta^{15}N$-NO_3^-, $\delta^{15}N$-DIN, or $\delta^{15}N$ biogenic N_2 as a function of f_{2bioN2} are shown in Fig. 6. Surprisingly, ε values estimated from the slope of these relationships are not sensitive to choice of method for calculating f despite the lack of 1:1 correspondence between different bases ($Np_{expected}$, biogenic N_2, or DIN; Fig. 9). In the case of ε calculated from changes in $\delta^{15}N$-DIN, ε ranged narrowly with choice of f from 6.3 to 7.4 with standard errors on the slope of < 0.6 (Table 1). As there was no significant difference between bases for calculating f, it appears that all three of our approaches are valid for this purpose.

BGD
12, 7257–7299, 2015

However, ε for N-loss (closed system) does vary significantly between calculations using changes in δ^{15}N-NO_3^-, δ^{15}N-DIN, or δ^{15}N biogenic N_2. ε is largest for changes in δ^{15}N-NO_3^- ($\sim$ 14 ‰) and smallest for changes in δ^{15}N-DIN ($\sim$ 7 ‰). ε based on δ^{15}N biogenic N_2 is intermediate ($\sim$ 11 ‰). The latter two using DIN or biogenic N_2 as the basis to calculate ε, are likely more realistic, being more consistent with mass balance considerations (Bourbonnais et al., 2015). Calculations based on changes in δ^{15}N-NO_3^- are affected by NO_2^- accumulation and isotope effects of NO_2^- oxidation (see above). The 4 ‰ difference in ε calculated from changes in δ^{15}N of biogenic N_2 vs. δ^{15}N of DIN may arise from the contribution of NH_4^+ derived from organic matter to biogenic N_2 via the anammox process.

The different approaches for estimating the ε for N-loss can also be evaluated by examining the initial substrate δ^{15}N predicted where $f = 0$ for each set of regressions. In the case of changes in δ^{15}N-DIN and using $Np_{expected}$ or biogenic N_2 as bases for f, realistic values are found consistent with the source of upwelled waters of 6 to 7 ‰ (Ryabenko et al., 2012; Table 1). For regressions based on changes in δ^{15}N-biogenic N_2, initial δ^{15}N values are somewhat lower ($\sim$ 3 ‰), also possibly due to a source from organic N decomposition.

Estimates of ε using open system equations are generally much higher than for closed system equations particularly for changes in δ^{15}N-NO_3^- with unrealistically high values (39–63 ‰; Table 2). However, values for both closed and open systems tended to converge for estimates based on changes in δ^{15}N-DIN or biogenic N_2 δ^{15}N with the latter having no significant difference (Fig. 10). Estimates of substrate initial δ^{15}N using the open system equations range widely and do not consistently reflect realistic values (Table 2).

Closed system estimates of ε are likely more reliable in our setting because of low likelihood of mixing between water masses of contrasting characteristics. Temperature and salinity in the OMZ at our stations ranged mostly from 13.5 to 15 °C and 34.88 to 34.98 (Fig. 2), suggestive of a single water mass (with little influence from mixing with

BGD
12, 7257–7299, 2015

other water mass). Accordingly, as in Bourbonnais et al. (2015), we view the closed system equations as most reliable with a value of ~ 6.5 ‰ for ε based on changes in δ^{15}N DIN as the likely best estimate. However, given the overlap with the results of open system equations for changes in δ^{15}N of biogenic N_2, an upper bound of ~ 11 ‰ appears appropriate. This range in ε for N-loss falls below the results of Bourbonnais et al. (2015) for a near-coastal eddy in the same region and time period (~ 14 ‰) and much less than the canonical range of 20 to 30 ‰.

There are several reasonable explanations for these relatively low ε values. These include higher microbial growth rates associated with higher productivity which would shift biochemical rate limitation away from enzyme reactions to membrane transport with low fractionation potential (e.g. Wada and Hattori, 1978). Another is greater influence from benthic N cycling processes in our relatively shallow inshore system as compared to deeper waters. Sediment N-loss has been shown to incur low ε due to, in analogous fashion to the affect of microbial growth rate, dominance of substrate transport limitation through the sediment (Brandes and Devol, 1997). This possibility will be explored further in the next section. Unlikely explanations for our relatively low ε values for N-loss include the effects of decreasing NO_3^- concentration (Kritee et al., 2012) and contributions from organic N via anammox to biogenic N_2. Lack of curvature in the Rayleigh plots demonstrates a lack of dependence of substrate concentration (Fig. 6a and b) as the range in f corresponds to a large range in NO_3^- or DIN concentrations. The possible effects of contributions from organic N to biogenic N_2 has already been taken into account in calculations based on changes in the δ^{15}N of biogenic N_2.

4.3 Using ε values for estimating sediment N-loss

As discussed above, the low ε value we observe for water column N-loss at our inshore stations may be explained by contributions from sediment N-loss (e.g. see Sigman et al., 2003). If so, observed ε for N-loss in the water-column should be the weighted

BGD
12, 7257–7299, 2015

average of the actual ε values for N-loss in the water column and sediments:

$$\varepsilon_{obs} = \varepsilon_{wc} \times (1 - P_{sed}) + \varepsilon_{sed} \times P_{sed} \quad (12)$$

where ε_{wc} and ε_{sed} are the isotope effect of water column and sediments and P_{sed} is the proportion of water column and sedimentary N-loss, respectively. We take 6.5 ‰ as the value for ε_{obs} (Fig. 6, Table 1), a value of 14 ‰ for ε_{wc} as estimated for offshore waters by Bourbonnais et al. (2015), and a ε_{sed} of 1.5 ‰ as in Sigman et al. (2003). From these numbers, we estimated that the proportion of N-loss due to sedimentary N-loss could be up to 60 % at our coastal stations, which is in the same range than previously reported for other marine coastal environments, e.g. Saanich Inlet (also up to 60 %; Bourbonnais et al., 2013). Our estimate is however higher than the 25 % of benthic vs. total N-loss from a reaction-diffusion model and direct flux measurements for the same coastal region off Peru (Kalvelage et al., 2013). However, direct measurements of fluxes at single locations over relatively short time periods likely underestimate fluxes due to spatial and temporal heterogeneity associated with N-flux hotspots.

5 Conclusions

The inshore Peru OMZ is distinguished from offshore by its high productivity as a consequence of coastal upwelling as well as possible greater influence from benthic processes. To examine impact on N-loss processes and their isotope effects, we investigated the dynamics of N and O isotope of NO_2^- and NO_3^- at 6 coastal stations off Peru.

We found that N-loss processes produced large variations in isotopic composition. NO_2^- $\delta^{15}N$ ranged from –20 to 10 ‰ and NO_3^- $\delta^{15}N$ ranged from 10 to 50 ‰. Generally, NO_3^- and NO_2^- isotope values varied inversely with their concentrations as expected for Rayleigh-like fractionation effects. Isotope values were usually higher in low-O_2 near bottom waters where concentrations were also relatively low.

BGD
12, 7257–7299, 2015

We observed, for the first time, a positive linear relationship between NO_2^- $\delta^{15}N$ and $\delta^{18}O$ at our inshore stations. In offshore OMZ waters, such a relationship has never previously been observed as NO_2^- $\delta^{18}O$ reflected equilibration with water in these regions (Buchwald and Casciotti, 2013). Our results suggest a turnover time for NO_2^- faster than the equilibration time with water and the dominance of NO_2^- reduction over NO_2^- oxidation in these highly productive coastal waters. We estimated a NO_2^- turnover time of at least ~ 40 days from our data.

The difference in $\delta^{15}N$ between NO_3^- and NO_2^- $\Delta(\delta^{15}N)$ was high, reaching up to 40 ‰ in deeper waters and greater than expected from NO_3^- and NO_2^- reduction only. The influence of NO_2^- oxidation is consistent with this observation due to its inverse fractionation effect (Casciotti, 2009). Additional evidence for NO_2^- oxidation is found in the relationship between NO_3^- $\delta^{15}N$ and $\delta^{18}O$. NO_3^- reduction alone is expected to produce a 1:1 relationship (Granger et al., 2008). While we observed a linear relationship between NO_3^- $\delta^{15}N$ and $\delta^{18}O$, the slope of 0.86 is indicative of simultaneous addition of NO_3^- with relatively low $\delta^{18}O$, also consistent with a role for NO_2^- oxidation at our coastal sites. However, a favorable thermodynamic couple for NO_2^- oxidation in the absence of O_2 in these waters remains unknown.

A number of different approaches for estimating ε for N-loss were compared including choice of N form for changes in $\delta^{15}N$ (NO_3^-, DIN, or biogenic N_2), closed vs. open system Rayleigh equations, and the basis for calculating the denominator in f ($Np_{expected}$, DIN + biogenic N_2, or maximum NO_3^-). For the latter, there was little difference in estimated ε despite discrepancies between the removal of NO_3^- and appearance of N_2 estimated from them. Observation of a single water mass (T–S plot) in our coastal region as well as more realistic ranges for derived ε and initial $\delta^{15}N$ indicated that closed system assumptions were more realistic. Using closed system equations, relatively low ε values were calculated; ~ 7 ‰ for changes in the $\delta^{15}N$ of DIN and ~ 11 ‰ for changes in the $\delta^{15}N$ of biogenic N_2. As in Bourbonnais et al. (2015), ε cal-

BGD
12, 7257–7299, 2015

culated from changes in the $\delta^{15}N$ of NO_3^- alone was not representative of the ε for overall N-loss in consideration of the build up of NO_2^- with distinct $\delta^{15}N$. These estimates for ε for net N-loss are lower than recently reported for a nearby offshore eddy with intense N-loss (~ 14 ‰; Bourbonnais et al., 2015). This lower ε may be attributed to the influence of sedimentary N-loss, with a highly suppressed ε, on the overlying water column at our shallow stations. Given this assumption, we estimate that sedimentary N-loss (by both denitrification and anammox) could account for up to 60 % of the total N-loss in in shore Peru OMZ waters.

Our results further support geographical variations in the ε of N-loss in OMZ'S, possibly related to the effects of varying primary productivity and microbial growth rates on the expression of ε and partitioning between water-column and sedimentary denitrification. These variations need to be considered in future global isotopic N budget (e.g. see Brandes and Devol, 2002), potentially bringing the global N budget more in balance. This is further supported by the relatively lower ε for N-loss recently observed offshore in the ETSP OMZ by Bourbonnais et al. (2015), where most of the N-loss occurs. A lower water-column ε for N-loss also decreases the fraction of sedimentary denitrification needed to balance the global isotopic N budget (Brandes and Devol, 2002; Altabet, 2007).

Acknowledgements. This research was supported by the Deutsche Forschungsgemeinschaft-project SFB-754 (www.sfb754.de), SOPRAN II (grant # FKZ 03F0611A; www.sopran.pangaea.de), the Nitrogen Isotope and N_2/Ar Biogeochemistry of the Peru Suboxic Zone project (National Science Foundation award OCE-0851092), the University of Massachusetts Intercampus Marine Science graduate program support to H. Hu and a NSERC Postdoctoral Fellowship to A.B. We would like to thank the captain and crew of R/V *Meteor* during the M91 cruise and Daniel Kiefhaber, Avi Bernales and Violeta Leon for their help during sampling and/or sample analysis. We thank the authorities of Peru for the permission to work in their territorial waters.

BGD
12, 7257–7299, 2015

References

Alkhatib, M., Lehmann, M. F., and del Giorgio, P. A.: The nitrogen isotope effect of benthic remineralization-nitrification-denitrification coupling in an estuarine environment, Biogeosciences, 9, 1633–1646, doi:10.5194/bg-9-1633-2012, 2012.

Altabet, M. A.: Isotopic tracers of the marine nitrogen cycle: present and past, in: The Handbook of Environmental Chemistry, vol. 2, edited by: Hutzinger, O., Springer-Verlag, Berlin Heidelberg, 251–293, 2005.

Altabet, M. A.: Constraints on oceanic N balance/imbalance from sedimentary ^{15}N records, Biogeosciences, 4, 75–86, doi:10.5194/bg-4-75-2007, 2007.

Altabet, M. A. and Francois, R.: Sedimentary nitrogen isotopic ratio as a recorder for surface ocean nitrate utilization, Global Biogeochem. Cy., 8, 103–116, 1994.

Altabet, M. A., Francois, R., Murray, D. W., and Prell, W. L.: Climate-related variations in denitrification in the Arabian Sea from sediment $^{15}N/^{14}N$ ratios, Nature, 373, 506–509, 1995.

Andersson, K. K. and Hooper, A. B.: O_2 and H_2O are each the source of one O in NO_2^- produced from NH_3 by Nitrosomonas: ^{15}N-NMR evidence, FEBS Lett., 164, 236–240, 1983.

Babbin, A. R., Keil, R. G., Devol, A. H., and Ward, B. B.: Organic matter stoichiometry, flux, and oxygen control nitrogen loss in the ocean, Science, 344, 406–408, 2014.

Bourbonnais, A., Lehmann, M. F., Waniek, J. J., and Schulz-Bull, D. E.: Nitrate isotope anomalies reflect N_2 fixation in the Azores Front Region (subtropical NE Atlantic), J. Geophys. Res.-Oceans, 114, C03003, doi:10.1029/2007JC004617, 2009.

Bourbonnais, A., Lehmann, M. F., Hamme, R. C., Manning, C. C, and Kim Juniper, S.: Nitrate elimination and regeneration as evidenced by dissolved inorganic nitrogen isotopes in Saanich Inlet, a seasonally anoxic fjord, Mar. Chem., 157, 194–207, 2013.

Bourbonnais, A., Altabet, M. A., Charoenpong, C. N., Larkum, J., Hu, H., Bange, H. W., and L. Stramma: N-loss isotope effects in the Peru oxygen minimum zone studied using a mesoscale eddy as a natural tracer experiment, Global Biogeochem. Cy., 29, doi:10.1002/2014GB005001, 2015.

Brandes, J. A. and Devol, A. H.: Isotopic fractionation of oxygen and nitrogen in coastal marine sediments, Geochim. Cosmochim. Ac., 61, 1793–1801, 1997.

Brandes, J. A. and Devol, A. H.: A global marine-fixed nitrogen isotopic budget: implications for Holocene nitrogen cycling, Global Biogeochem. Cy., 16, 67-1–67-14, 2002.

BGD
12, 7257–7299, 2015

Brandes, J. A., Devol, A. H., Yoshinari, T., Jayakumar, D. A., and Naqvi, S. W. A.: Isotopic composition of nitrate in the central Arabian Sea and eastern tropical North Pacific: a tracer for mixing and nitrogen cycles, Limnol. Oceanogr., 43, 1680–1689, 1998.

Brunner, B., Contreras, S., Lehmann, M. F., Matantseva, O., Rollog, M., Kalvelage, T., Klockgether, G., Lavik, G., Jetten, M. S. M., Kartal, B., and Kuypers, M. M. M: Nitrogen isotope effects induced by anammox bacteria, P. Natl. Acad. Sci. USA, 110, 18994–18999, 2013.

Bryant, J. P., Chapin, F. S., and Klein, D. R.: Carbon uutrient balance of boreal plants in relation to vertebrate herbivory, Oikos, 40, 357–368, 1983.

Buchwald, C. and Casciotti, K. L.: Oxygen isotopic fractionation and exchange during bacterial nitrite oxidation, Limnol. Oceanogr., 55, 1064–1074, 2010.

Buchwald, C. and Casciotti, K. L.: Isotopic ratios of nitrite as tracers of the sources and age of oceanic nitrite, Nat. Geosci., 6, 308–313, 2013.

Casciotti, K. L.: Inverse kinetic isotope fractionation during bacterial nitrite oxidation, Geochim. Cosmochim. Ac., 73, 2061–2076, 2009.

Casciotti, K. L. and Buchwald, C.: Insights on the marine microbial nitrogen cycle from isotopic approaches to nitrification, Front. Microbiol., 3, 1–14, 2012.

Casciotti, K. L. and McIlvin, M. R.: Isotopic analyses of nitrate and nitrite from reference mixtures and application to eastern tropical North Pacific waters, Mar. Chem., 107, 184–201, 2007.

Casciotti, K. L., Sigman, D. M., Hastings, M. G., Böhlke, J. K., and Hilkert, A.: Measurement of the oxygen isotopic composition of nitrate in seawater and freshwater using the denitrifier method, Anal. Chem., 74, 4905–4912, 2002.

Casciotti, K. L., Böhlke, J. K., McIlvin, M. R., Mroczkowski, S. J., and Hannon, J. E.: Oxygen isotopes in nitrite: analysis, calibration, and equilibration, Anal. Chem., 79, 2427–2436, 2007.

Casciotti, K. L., McIlvin, M., and Buchwald, C.: Oxygen Isotopic Exchange and Fractionation during Bacterial Ammonia Oxidation, Limnol. Oceanogr., 55, 753–762, 2010.

Casciotti, K. L., Buchwald, C., and McIlvin, M.: Implications of nitrate and nitrite isotopic measurements for the mechanisms of nitrogen cycling in the Peru oxygen deficient zone, Deep-Sea Res. Pt. I, 80, 78–93, 2013.

Chang, B. X., Devol, A. H., and Emerson, S. R.: Denitrification and the nitrogen gas excess in the eastern tropical South Pacific oxygen deficient zone, Deep-Sea Res. Pt. I, 57, 1092–1101, 2010.

BGD
12, 7257–7299, 2015

Cline, J. D. and Kaplan, I. R.: Isotopic fractionation of dissolved nitrate during denitrification in the eastern tropical North Pacific ocean, Mar. Chem., 3, 271–299, 1975.
Charoenpong, C. N., Bristow, L. A., and Altabet, M. A.: A continuous flow isotope ratio mass spectrometry method for high precision determination of dissolved gas ratios and isotopic composition, Limnol. Oceanogr. Meth., 12, 323–337, 2014.
Codispoti, L. A.: An oceanic fixed nitrogen sink exceeding 400 Tg N a^{-1} vs. the concept of homeostasis in the fixed-nitrogen inventory, Biogeosciences, 4, 233–253, doi:10.5194/bg-4-233-2007, 2007.
Codispoti, L. A. and Christensen, J. P.: Nitrification, denitrification and nitrous oxide cycling in the eastern tropical South Pacific ocean, Mar. Chem., 16, 277–300, 1985.
Codispoti, L. A., Friederich, G. E., Packard, T. T., Glover, H. E., Kelly, P. J., Spinrad, R. W., and Barber, R. T.: High nitrite levels off northern Peru: a signal of instability in the marine denitrification rate, Science, 233, 1200–1202, 1986.
Dalsgaard, T., Stewart, F. J., Thamdrup, B., Brabandere, L. D., Revsbech, P., and Ulloa, O.: Oxygen at nanomolar levels reversibly suppresses process rates and gene expression in anammox and denitrification in the oxygen, mBio, 5, e01966-14, doi:10.1128/mBio.01966-14, 2014.
Dore, J. E. and Karl, D. M.: Nitrification in the euphotic zone as a source for nitrite, nitrate, and nitrous oxide at station ALOHA, Limnol. Oceanogr., 41, 1619–1628, 1996.
Emerson, S., Stump, C., Wilbur, D., and Quay, P.: Accurate measurement of O_2, N_2, and Ar gases in water and the solubility of N_2, Mar. Chem., 64, 337–347, 1999.
Falkowski, P. G.: Evolution of the nitrogen cycle and its influence on the biological sequestration of CO_2 in the ocean, Nature, 387, 272–275, 1997.
Friedman, S. H., Massefski, W., and Hollocher, T. C.: Catalysis of intermolecular oxygen atom transfer by nitrite dehydrogenase of Nitrobacter agilis, J. Biol. Chem., 261, 10538–10543, 1986.
Füssel, J., Lam, P., Lavik, G., Jensen, M. M., Holtappels, M., Günter, M., and Kuypers, M. M. M.: Nitrite oxidation in the Namibian oxygen minimum zone, ISME J., 6, 1200–1209, 2012.
Granger, J. and Sigman, D. M.: Removal of nitrite with sulfamic acid for nitrate N and O isotope analysis with the denitrifier method, Rapid Commun. Mass Sp., 23, 3753–3762, 2009.
Granger, J., Sigman, D. M., Needoba, J. A., and Harrison, P. J.: Coupled nitrogen and oxygen isotope fractionation of nitrate during assimilation by cultures of marine phytoplankton, Limnol. Oceanogr., 49, 1763–1773, 2004.

BGD
12, 7257–7299, 2015

Granger, J., Sigman, D. M., Lehmann, M. F., and Tortell, P. D.: Nitrogen and oxygen isotope fractionation during dissimilatory nitrate reduction by denitrifying bacteria, Limnol. Oceanogr., 53, 2533–2545, 2008.

Gruber, N.: The dynamics of the marine nitrogen cycle and its influence on atmospheric CO_2 variations, in: The Ocean Carbon Cycle and Climate, edited by: Follows, M. and Oguz, T., Kluwer Academic, Dordrecht, the Netherlands, 97–148, 2004.

Gruber, N.: The marine nitrogen cycle: overview of distributions and processes, in: Nitrogen in the Marine Environment, 2nd ed., edited by: Capone, D. G., Bronk, D. A., Mulholland, M. R., and Carpenter, E. J., Elsevier, Amsterdam, 1–50, 2008.

Hamme, R. C.: Mechanisms controlling the global oceanic distribution of the inert gases argon, nitrogen and neon, Geophys. Res. Lett., 29, 35-1–35-4, 2002.

Kalvelage, T., Lavik, G., Lam, P., Contreras, S., Arteaga, L., Loscher, C. R., Oschlies, A., Paulmier, A., Stramma, L., and Kuypers, M. M. M.: Nitrogen cycling driven by organic matter export in the South Pacific oxygen minimum zone, Nat. Geosci., 6, 228–234, 2013.

Kritee, K., Sigman, D. M., Granger, J., Ward, B. B., Jayakumar, A., and Deutsch, C.: Reduced isotope fractionation by denitrification under conditions relevant to the ocean, Geochim. Cosmochim. Ac., 92, 243–259, 2012.

Kuypers, M. M. M., Sliekers, A. O., Lavik, G., Schmid, M., Jørgensen, B. B., Kuenen, J. G., Sinninghe Damsté, J. S., Strous, M., and Jetten, M. S. M.: Anaerobic ammonium oxidation by anammox bacteria in the Black Sea, Nature, 422, 608–611, 2003.

Kuypers, M. M., Lavik, G., Woebken, D., Schmid, M., Fuchs, B. M., Amann, R., Jørgensen, B. B., and Jetten, M. S. M.: Massive nitrogen loss from the Benguela upwelling system through anaerobic ammonium oxidation, P. Natl. Acad. Sci. USA, 102, 6478–6483, 2005.

Lam, P., Lavik, G., Jensen, M. M., van de Vossenberg, J., Schmid, M., Woebken, D., Gutiérrez, D., Amann, R., Jetten, M. S. M., and Kuypers, M. M. M.: Revising the nitrogen cycle in the peruvian oxygen minimum zone, P. Natl. Acad. Sci. USA, 106, 4752–4757, 2009.

Lam, P., Jensen, M. M., Kock, A., Lettmann, K. A., Plancherel, Y., Lavik, G., Bange, H. W., and Kuypers, M. M. M.: Origin and fate of the secondary nitrite maximum in the Arabian Sea, Biogeosciences, 8, 1565–1577, doi:10.5194/bg-8-1565-2011, 2011.

Lehmann, M. F., Sigman, D. M., McCorkle, D. C., Granger, J., Hoffmann, S., Cane, G., and Brunelle, B. G.: The distribution of nitrate $^{15}N/^{14}N$ in marine sediments and the impact of benthic nitrogen loss on the isotopic composition of oceanic nitrate, Geochim. Cosmochim. Ac., 71, 5384–5404, 2007.

BGD
12, 7257–7299, 2015

Liu, K. K.: Geochemistry of inorganic nitrogen compounds in two marine environments: the Santa Barbara Basin and the ocean off of Peru, Ph.D. thesis, University of California, Los Angeles, 1979.
Lomas, M. W. and Lipschultz, F.: Forming the primary nitrite maximum: nitrifiers or phytoplankton?, Limnol. Oceanogr., 51, 2453–2467, 2006.
Mariotti, A., Germon, J. C., Hubert, P., Kaiser, P., Letolle, R., Tardieux, A., and Tardieux, P.: Experimental determination of nitrogen kinetic isotope fractionation: some principles; illustration for the denitrification and nitrification processes, Plant Soil, 62, 413–430, 1981.
McIlvin, M. R. and Altabet, M. A.: Chemical conversion of nitrate and nitrite to nitrous oxide for nitrogen and oxygen isotopic analysis in freshwater and seawater, Anal. Chem., 77, 5589–5595, 2005.
McIlvin, M. R. and Casciotti, K. L.: Method for the analysis of $\delta^{18}O$ in water, Anal. Chem., 78, 2377–2381, 2006.
Reed, D. C., Slomp, C. P., and Gustafsson, B. G.: Sedimentary phosphorus dynamics and the evolution of bottom-water hypoxia: a coupled benthic–pelagic model of a coastal system, Limnol. Oceanogr., 56, 1075–1092, 2011.
Richards, F. A. and Benson, B. B.: Nitrogen/argon and nitrogen isotope ratios in two anaerobic environments, the Cariaco Trench in the Caribbean Sea and Dramsfjord, Norway, Deep-Sea Res., 7, 254–264, 1961.
Sigman, D. M., Casciotti, K. L., Andreani, M., Barford, C., Galanter, M., and Bohlke, J. K.: A bacterial method for the nitrogen isotopic analysis of nitrate in seawater and freshwater, Anal. Chem., 73, 4145–4153, 2001.
Sigman, D. M., Robinson, R., Knapp, A. N., Van Geen, A., McCorkle, D. C., Brandes, J. A., and Thunell, R. C.: Distinguishing between water column and sedimentary denitrification in the Santa Barbara Basin using the stable isotopes of nitrate, Geochem. Geophy. Geosy., 4, 1040, doi:10.1029/2002GC000384, 2003.
Sigman, D. M., Granger, J., DiFiore, P. J., Lehmann, M. M., Ho, R., Cane, G., and Van Geen, A.: Coupled nitrogen and oxygen isotope measurements of nitrate along the eastern North Pacific margin, Global Biogeochem. Cy., 19, GB4022, doi:10.1029/2005GB002458, 2005.
Stramma, L., Bange, H. W., Czeschel, R., Lorenzo, A., and Frank, M.: On the role of mesoscale eddies for the biological productivity and biogeochemistry in the eastern tropical Pacific Ocean off Peru, Biogeosciences, 10, 7293–7306, doi:10.5194/bg-10-7293-2013, 2013.

BGD
12, 7257–7299, 2015

Strous, M., Pelletier, E., Mangenot, S., Rattei, T., Lehner, A., Taylor, M. W., and Horn, M.: Deciphering the evolution and metabolism of an anammox bacterium from a community genome, Nature, 440, 790–794, 2006.

Voss, M., Dippner, J. W., and Montoya, J. P.: Nitrogen isotope patterns in the oxygen-deficient waters of the eastern tropical North Pacific ocean, Deep-Sea Res. Pt. I, 48, 1905–1921, 2001.

Wada, E. and Hattori, A.: Nitrogen isotope effects in the assimilation of inorganic compounds by marine diatoms, Geomicrobiol J., 1, 85–101, 1978.

Ward, B. B., Devol, A. H., Rich, J. J., Chang, B. X., Bulow, S. E., Naik, H., Pratihary, A., and Jayakumar, A.: Denitrification as the dominant nitrogen loss process in the Arabian Sea, Nature, 461, 78–81, 2009.

BGD
12, 7257–7299, 2015

Table 1. ε for NO_3^- reduction and net N loss estimated from both DIN consumption and produced biogenic N_2 using Rayleigh closed system equations (Eqs. 1 and 2). Results are calculated for f based on either $Np_{expected}$ (Eq. 5), biogenic N_2 (Eq. 10) and measured substrate divided by maximum (upwelled) substrate concentrations (see text, Sect. 2.4).

	Basis for f	ε	y-Intercept	r^2	Error on slope
δ^{15}N-NO_3^-	$Np_{expected}$	13.89	3.74	0.92	0.71
	N_2 Biogenic	14.27	3.71	0.95	0.86
	$[NO_3^-]/[NO_3]_{max}$	14.66	−0.55	0.95	0.56
δ^{15}N-DIN	$Np_{expected}$	6.32	7.20	0.92	0.33
	N_2 Biogenic	6.55	6.71	0.94	0.44
	DIN/DIN_{max}	7.44	10.90	0.91	0.59
δ^{15}N-Biogenic N_2	$Np_{expected}$	10.45	2.94	0.70	1.51
	N_2 Biogenic	10.56	3.04	0.72	1.49

BGD
12, 7257–7299, 2015

Table 2. ε for NO_3^- reduction, and net N loss estimated from both DIN consumption and produced biogenic N_2 using Rayleigh open system equations (Eqs. 3 and 4). Results are calculated for f based on either $Np_{expected}$ (Eq. 5), biogenic N_2 (Eq. 10) and measured substrate divided by maximum (upwelled) substrate concentrations (see text, Sect. 2.4).

	Basis for f	ε	y-Intercept	r^2	Error on slope
δ^{15}N-NO_3^-	$Np_{expected}$	62.97	−18.42	0.86	4.45
	N_2 Biogenic	66.30	−21.92	0.87	6.24
	$[NO_3^-]/[NO_3^-]_{max}$	38.89	6.19	0.87	2.66
δ^{15}N-DIN	$Np_{expected}$	17.35	3.26	0.88	1.19
	N_2 Biogenic	19.98	1.72	0.89	1.79
	DIN/DIN_{max}	13.22	8.45	0.91	0.92
δ^{15}N-Biogenic N_2	$Np_{expected}$	12.27	1.94	0.67	1.92
	N_2 Biogenic	14.15	2.25	0.68	2.17

BGD
12, 7257–7299, 2015

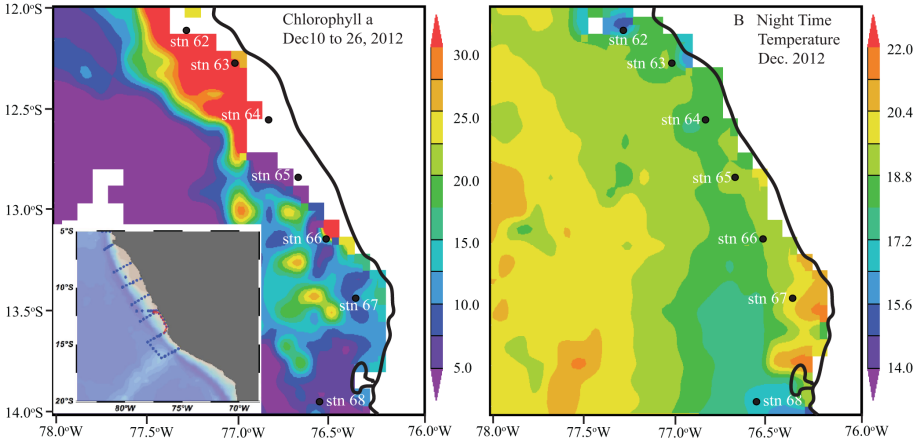

Figure 1. Station map with satellite data from http://disc.sci.gsfc.nasa.gov/giovanni/. **(a)** Sea surface chlorophyll a concentrations (mg m^{-3}). Insert map (produced by Ocean Data View software) shows all cruise stations; stations discussed in this paper are indicated by the red line and **(b)** night time sea surface temperature (°C).

BGD
12, 7257–7299, 2015

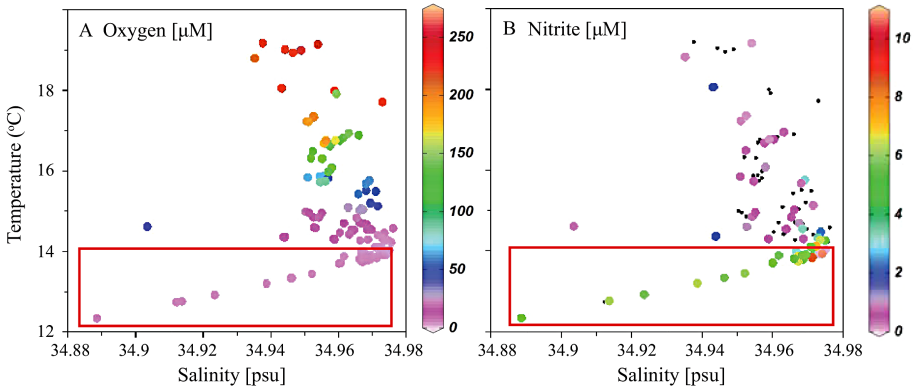

Figure 2. Temperature vs. salinity plots. In **(a)**, color indicates [O_2] (µM). In **(b)**, color indicates [NO_2^-] (µM). Points at bottom in red rectangle of each plot belong to station 68 for depths greater than 150 m. Black dots in **(b)** mean no [NO_2^-] data available.

BGD
12, 7257–7299, 2015

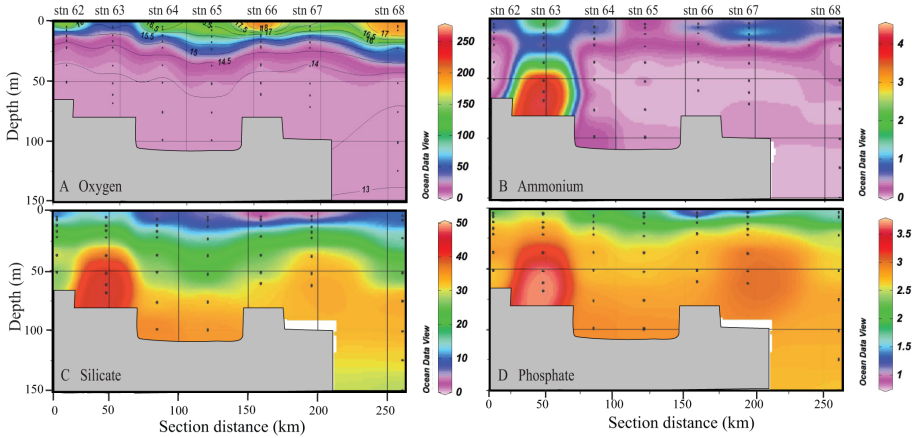

Figure 3. O_2 and nutrient distribution along the transect. **(a)** [O_2] (μM) with isotherm overlay and **(b)** [NH_4^+] (μM), **(c)** [$Si(OH)_4$] (μM) and **(d)** [PO_4^{3-}] (μM). Grey region represents bathymetry. The depth for station 68 is 253 m.

BGD
12, 7257–7299, 2015

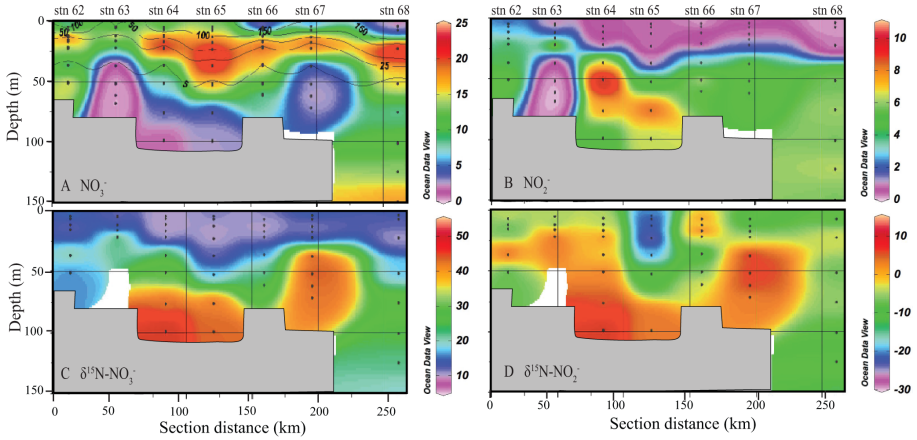

Figure 4. Transects off the Peru coast for **(a)** [NO_3^-] (μM) with O_2 overlay, **(b)** [NO_2^-] (μM), **(c)** δ^{15}N-NO_3^- (‰) and **(d)** δ^{15}N-NO_2^- (‰). Grey region represents approximate bathymetry. No isotopic data are available for the deeper samples collected at station 63, because [NO_3^-] and [NO_2^-] were below analytical limits (< 0.5 μM).

BGD
12, 7257–7299, 2015

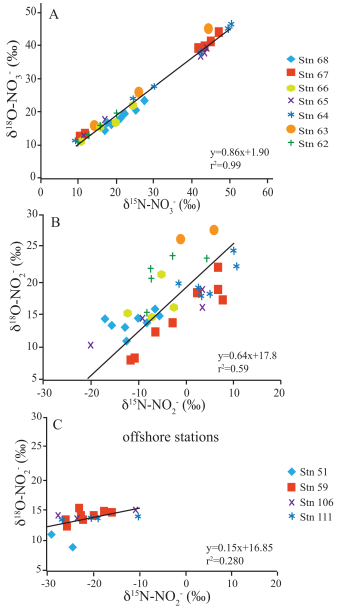

Figure 5. Relationships between $\delta^{15}N$ and $\delta^{18}O$ for NO_3^- and NO_2^-, respectively, for $O_2 \leq 10\,\mu M$. **(a)** $\delta^{18}O\text{-}NO_3^-$ vs. $\delta^{15}N\text{-}NO_3^-$ for station 62 to 68. **(b)** $\delta^{18}O\text{-}NO_2^-$ vs. $\delta^{15}N\text{-}NO_2^-$ for station 62 to 68. **(c)** $\delta^{18}O\text{-}NO_2^-$ vs. $\delta^{15}N\text{-}NO_2^-$ for M90 offshore stations 51, 59, 106 and 111 (see text, Sect. 3.3). For each plot, overall linear regressions are shown.

BGD
12, 7257–7299, 2015

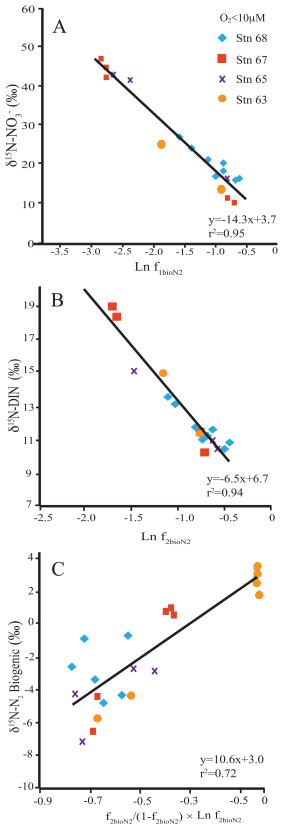

Figure 6. Raleigh relationships used to estimate ε (slope) and initial δ^{15}N-substrate (y-intercept) assuming a closed system. **(a)** for NO_3^- reduction (Eq. 1 and text, Sect. 2.4), **(b)** for N-loss calculated from the substrate (DIN) consumption (Eq. 1 and text, Sect. 2.4) and **(c)** for N-loss calculated from the δ^{15}N of biogenic N_2 (Eq. 2 and text, Sect. 2.4). In **(c)**, only samples with [O_2] less than 10 μM and biogenic N_2 values > 7.5 μM were considered.

BGD
12, 7257–7299, 2015

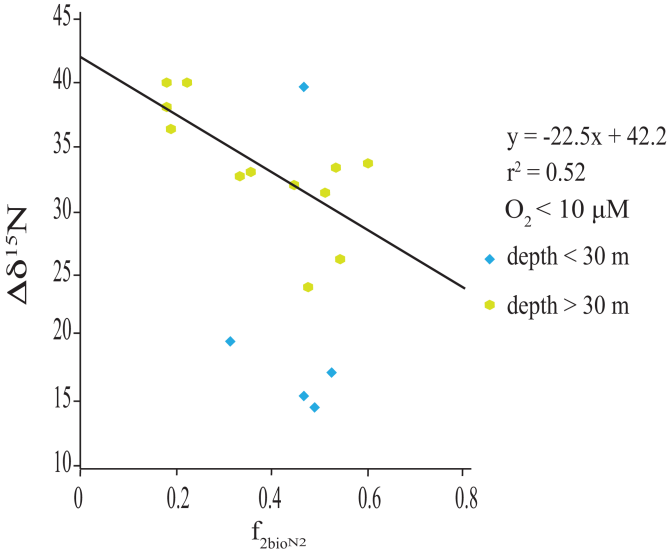

Figure 7. Relationship between $\Delta\delta^{15}N$ ($\Delta\delta^{15}N = \delta^{15}N\text{-}NO_3^- - \delta^{15}N\text{-}NO_2^-$) for waters with $O_2 < 10\,\mu M$ and f_2 based on biogenic N_2 (f_{2bioN2}). Points are distinguished by depth (< and > 30 m). Only data for biogenic N_2 values > 7.5 µM were considered.

BGD
12, 7257–7299, 2015

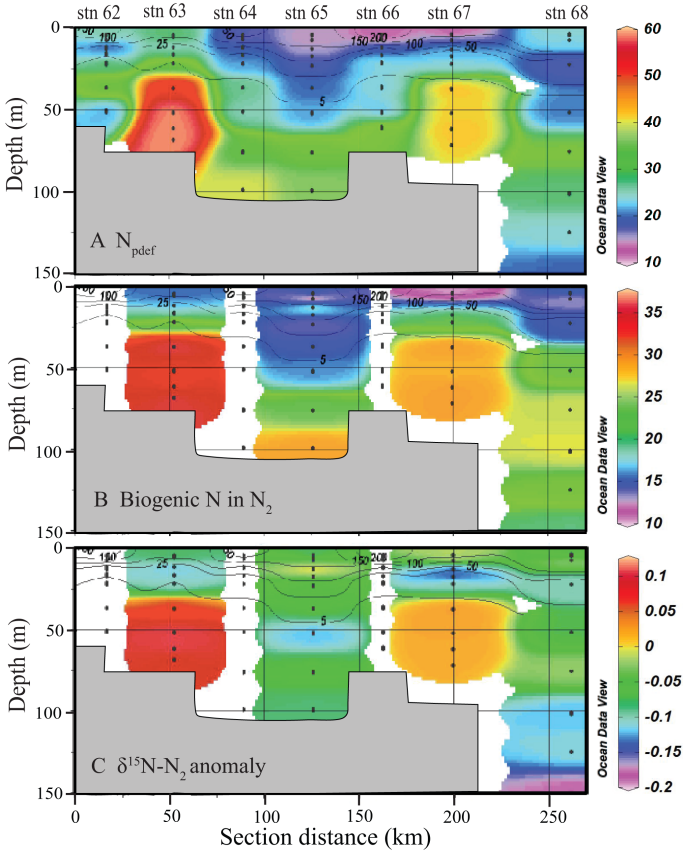

Figure 8. N deficit, biogenic N in N_2 and δ^{15}N-N_2 with O_2 overlaid. **(a)** N deficit calculated using PO_4^{3-} (μM) (N_{pdef}) and assuming Redfield stoichiometry (see Eqs. 6–8, Sect. 2.4). **(b)** biogenic N in N_2 (μM). **(c)** δ^{15}N-N_2 anomaly relative to equilibrium with atmosphere (‰). Biogenic N_2 or δ^{15}N-N_2 anomaly were not measured at stations 62, 64 and 66.

BGD
12, 7257–7299, 2015

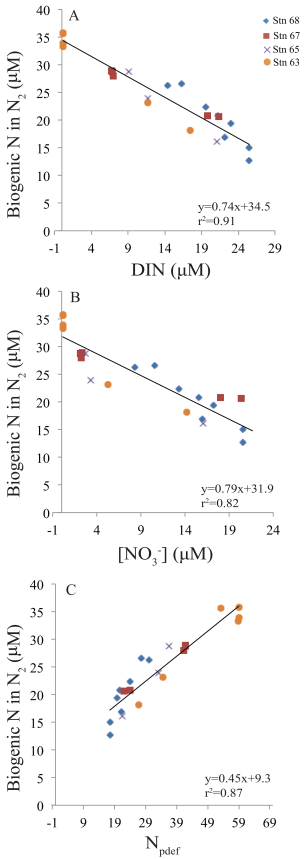

Figure 9. Cross-plots of biogenic N in N_2 vs. DIN **(a)**, NO_3^- **(b)** and Np_{def} (**c**, see Eqs. 6 to 8 in text). All plots have the overall linear regression overlaid. All the points are restricted to $[O_2]<$ 10 μM. Biogenic N_2 was not measured for stations 62, 64 and 66.

BGD
12, 7257–7299, 2015

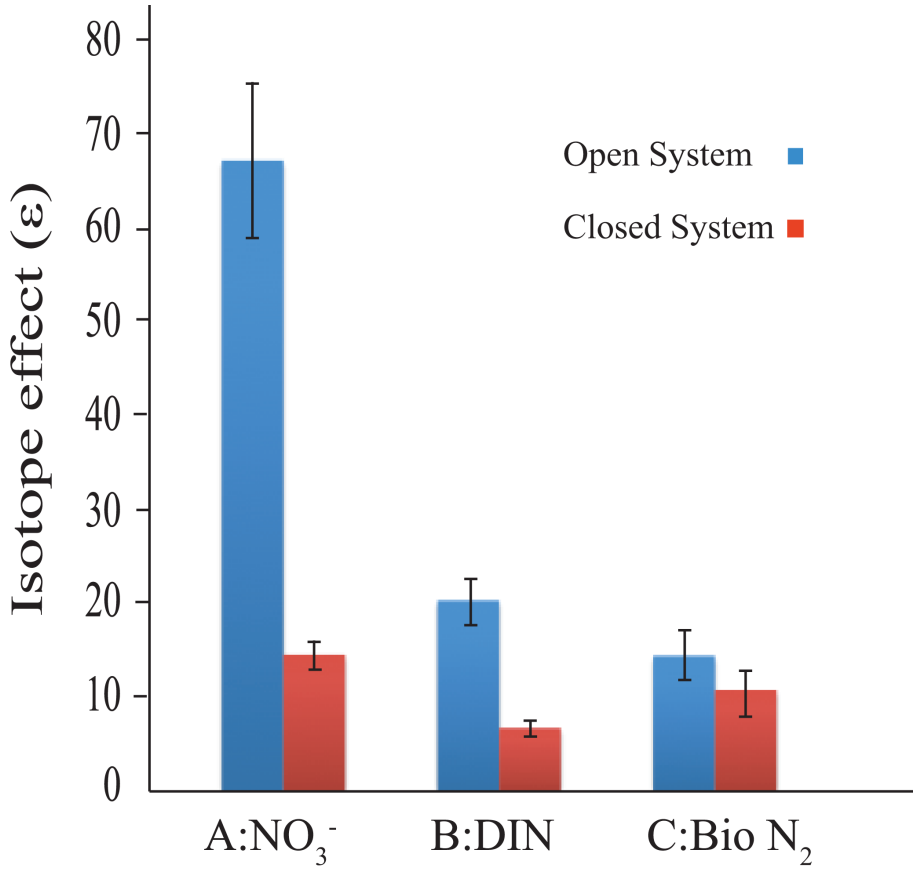

Figure 10. Comparison of ε estimated using closed vs. open system equations. Error bars (calculated errors on the slopes) are shown. Also compared are ε values calculated for changes in the $\delta^{15}N$ of either NO_3^- (A), DIN (B), or biogenic N_2 (C). For simplicity, ε values shown use f based on biogenic N_2. See Tables 1 and 2 for influence of other bases.

BGD
12, 7257–7299, 2015